# Molecular Lens of the Nonresonant Dipole Force

Bum Suk Zhao,[1] Hoi Sung Chung,[1] Keunchang Cho,[1] Sung Hyup Lee,[1] Sungu Hwang,[1] Jongwan Yu,[1] Y. H. Ahn,[2] J. Y. Sohn,[2] D. S. Kim,[2] Wee Kyung Kang,[3] and Doo Soo Chung[1,*]

[1]*School of Chemistry, Seoul National University, Seoul 151-747, Korea*
[2]*School of Physics, Seoul National University, Seoul 151-747, Korea*
[3]*Department of Chemistry, Soongsil University, Seoul 156-743, Korea*

(Received 13 December 1999)

A cylindrical molecular lens is formed by focusing a nanosecond IR laser pulse. Trajectories of a $CS_2$ molecular beam deflected by the lens are traced using the velocity map imaging technique. The characteristic lens parameters including the focal length, minimum beam width, and distance to the minimum-width position are determined. The laser intensity dependence of the parameters is in good agreement with theoretical predictions. Exciting possibilities for molecular optics and a new type of optical chromatography are opened up.

PACS numbers: 32.80.Lg, 33.80.Ps, 42.50.Vk

During the past decades tremendous effort has been expended in order to control the external degrees of freedom of particles using the mechanical forces of light. For two extreme cases, optical manipulation of particles has been achieved. Optical tweezers made of a focused laser beam can guide micron-sized particles [1], such as single DNA molecules [2,3], proteins [4,5], and bacteria [6], which are large enough to refract many photons of the laser field. At the other extreme, by absorbing and emitting many photons of near-resonant laser fields, atoms of simple quantum structures can be cooled below $\mu$K [7] and then trapped in a sufficiently confined region in space to achieve the phase space density needed for Bose-Einstein condensation [8]. Light forces have also initiated a new era of atomic optics by collimating and focusing atomic beams. Such developments in atomic optics have given rise to the birth of atomic interferometry [9], atomic lithography [10], and optical lattices [11]. However, for ordinary molecules, neither of the two schemes works. Regular molecules are too small to refract the laser beam geometrically. Unlike atoms, their complex vibrational and rotational level structures prevent them from absorbing and emitting photons repeatedly for efficient cooling [12].

Recently, several approaches have been suggested for the manipulation of molecules using a mechanical force exerted by the interaction of an intense nonresonant laser field with the induced dipole moment. The magnitude of the light force on a molecule is proportional to the molecular polarizability and the gradient of laser intensity [13,14]. The possibility of spatial alignment and trapping of molecules by a laser was demonstrated by calculations [15]. An optical centrifuge for controlled spinning of molecules with strong infrared fields was proposed to separate isotopes by selectively dissociating homonuclear diatomic molecules [16]. Analogous to atomic optics, molecular optics using near-resonant or far-off-resonant laser fields has been proposed [17,18]. However, only a limited number of experiments have been reported on the optical control of neutral molecules. Deflection of linear molecules such as $I_2$ and $CS_2$ using the nonresonant dipole forces of a nanosecond laser pulse has been demonstrated by measuring the changes in the time of flight (TOF) of the multiphoton-ionized molecular ions [13,14]. Cesium dimers produced in a magneto-optical trap and transferred to an optical dipole trap were detected using photoionization and TOF spectroscopy [19]. Ultracold potassium molecules in electronic ground state were also produced and detected by using two-color resonance ionization [20]. The alignment of neutral iodine molecules by a strong nonresonant laser pulse was also observed [21]. Although the deflection of the molecular beam has been confirmed experimentally, the verification of the theoretically predicted molecular lens properties [17] is still lacking.

In this Letter, we report on the spatial imaging of molecules deflected by a cylindrical molecular lens consisting of a nonresonant laser beam. Neutral molecules deflected by the lens are ionized via resonance-enhanced multiphoton ionization (REMPI) [22], and their images are observed with the velocity map imaging technique [23,24]. The images of the deflected molecules are clearly separated from those of the undeflected molecules. In addition, by tracing the trajectories of the deflected molecules, we have determined the characteristic lens parameters including the focal length ($f$), minimum molecular beam width ($W$), and distance from the lens to the minimum-width beam position ($D$). The values obtained and their dependence on the laser intensity are in good agreement with theoretical predictions [17,25].

A schematic diagram of the experimental apparatus and our coordinate convention is presented in Fig. 1. A pulsed supersonic beam of $CS_2$ is formed by expanding 35 torr $CS_2$ in 2 atm Ar through a 0.5-mm-diam nozzle at a rate of 10 Hz. The beam moves along the $z$ axis through a 0.5-mm-diam skimmer and a 0.6-mm-diam pinhole at the center of the repeller electrode. After propagating 85 mm from the nozzle, molecules are crossed by a 7-ns (FWHM) IR (wavelength $\lambda = 1064$ nm) Nd:YAG laser pulse propagating along the $x$ axis. Its energy and polarization are

  

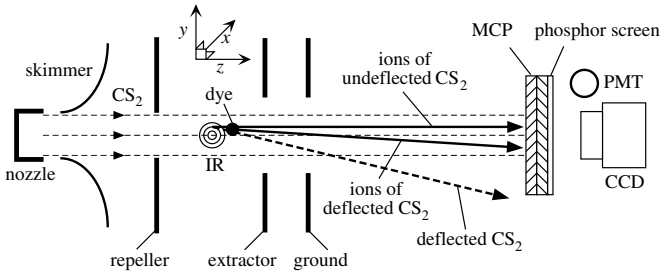


FIG. 1. Schematics showing the inside of the chamber, detectors, and the coordinate convention. The molecular beam propagates along the $z$ axis and the laser beam along the $x$ axis. Solid lines with arrowheads indicate trajectories of $CS_2$ molecules deflected by an IR laser pulse and then ionized by a dye laser pulse. The dashed line represents the trajectory of neutral $CS_2$ molecules deflected by the IR laser pulse.

adjusted by using a half-wave plate, Glan-laser polarizer, and Fresnel rhomb. The circularly polarized laser pulse is focused with an $f = 175$ mm convex lens. The molecular beam is then deflected toward the laser axis of highest intensity by the laser induced dipole force; the focused nonresonant laser beam is acting as a cylindrical lens for molecules. After a delay of 34 ns to avoid spatial and temporal overlapping between the IR and dye laser pulses, the deflected molecular beam is crossed by a 5-ns dye laser beam ($\lambda = 483$ nm) pumped by the third harmonics of the Nd:YAG laser. A 0.15-mJ dye laser pulse ionizes the deflected molecules mostly into molecular ions by the REMPI process of $[^2\Pi_{g3/2}]4p\sigma_u, (^3\Pi_u) \longleftarrow \tilde{X}^1\Sigma_g^+$ [22]. Since the mass of an electron is much smaller than that of a molecule, the momentum transfer from the dye laser to molecular ions during the REMPI process is minimal: $\vec{v}(CS_2) \approx \vec{v}(CS_2^+)$. Owing to the small waist radius ($\omega_0 \approx 10$ $\mu$m) of the ionizing dye laser of shorter wavelength and the (3 + 1)-photon REMPI process, the effective ionization volume is significantly smaller than the volume affected by the IR laser pulse.

The deflected and subsequently ionized molecules fly into a TOF tube along the molecular beam axis ($z$ axis) guided by a system of three electrode plates: a repeller, an extractor, and a ground. The respective distances from the repeller to the extractor and from the extractor to the ground are 35 and 15 mm. There is a 0.6-mm-diam pinhole on the repeller and there are 10-mm-diam holes at the centers of the extractor and the ground instead of the grids usually used in molecular fragmentation experiments [24]. When the ion image is focused on a 2D detector by using a combination of three gridless electrodes, ions of the same velocity are mapped onto the same position at the detector regardless of their initial positions. Note that although the focusing electrodes may affect the trajectories of ions, the spread and changes in transverse velocities, $\triangle v_y$, are not affected by the electrodes. This focusing electrode configuration performs velocity map imaging [23,24]. The blurring due to a finite ionization volume and distortions in the ionic trajectory induced by grid wires are removed. All the ions are transmitted. Consequently, the signal intensity and resolution of images focused by the gridless electrostatic lens system are dramatically enhanced. The focal length of the electrostatic lens is controlled by the ratio of the extractor voltage to the repeller voltage. For our chamber, a ratio of 2:3 produces optimal focusing.

After passing through the ground electrode, ions fly 650 mm to a microchannel plate (MCP) with a constant velocity. In order to detect molecular ions only, the MCP is gated with a negative high voltage pulse. Electrons emerging from the back of MCP impinge on a phosphor screen. The 2D emissions from the phosphor screen are recorded by a charge-coupled device camera. Images of molecular ions from 1800 laser shots are integrated and transferred to a computer for further analyses. Simultaneously, these emissions are detected by a photomultiplier tube, and displayed on a digital storage oscilloscope. This dual detection method is useful for optics alignment, MCP time gating, and ray tracing in which it is necessary to measure both the image shift and TOF.

In the presence of a nonresonant laser field propagating along the $x$ axis, the molecule-laser interaction is dominated by the Stark shift due to the induced dipole moment [13,26]

$$U(y,z,t) = -\frac{1}{4}\,\alpha E(y,z,t)^2, \tag{1}$$

where $\alpha$ is the static molecular polarizability and $E(y,z,t)$ is the space- and time-dependent pulse envelope. The resulting dipole force ($-\nabla U$) deflects the molecular rays traveling along the $z$ axis toward the laser axis of highest intensity. For a laser pulse with a Gaussian intensity profile propagating along the $x$ axis,

$$I = I_0 \exp[-(y^2 + z^2)/\omega_0^2] \exp(-4\ln 2 t^2/\tau^2), \tag{2}$$

where $I_0$, $\omega_0$, and $\tau$ are the peak intensity, waist radius, and duration of the pulse, respectively. The $y$-axis velocities of the molecular beam are changed according to [13]

$$\triangle v_y = \frac{\triangle Y}{\mathrm{TOF}} = -\frac{2\sqrt{2\pi}\, U_0 y \exp(-2y^2/\omega_0^2)}{m\omega_0 v_z \sqrt{1 + 2\ln 2[\omega_0/(v_z\tau)]^2}}, \tag{3}$$

where $\triangle Y$ is the image $y$ shift at the detector, $U_0$ the potential well depth formed by the molecule-laser interaction, and $m$ the mass of a molecule.

In Fig. 2 are illustrated two sets of images of the undeflected $CS_2$ molecular beam and the molecular beam deflected by the IR laser pulses ($I_0 = 5.0 \times 10^{11}$ W/cm$^2$), representing the first clear spatial separation of the deflected and undeflected molecular beams. The image obtained by focusing the ionizing dye laser beam 9 $\mu$m above (below) the IR laser axis is shifted 0.29 mm downward (upward). The images of undeflected molecular beams indicate that the initial transverse velocity spread is less than 4.8 m/s (FWHM). Since the dye laser samples a finite volume in space and time, the images of the

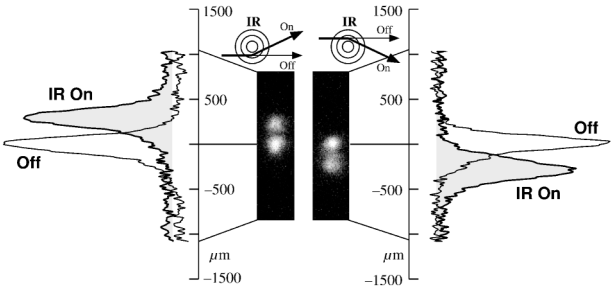


FIG. 2. Portion of the velocity-mapped ion images and their profiles for the deflected (IR On) and undeflected $CS_2$ molecules (Off). The vertical scale corresponds to the $y$ distance at the detector. Schemes show the relative locations of the foci of the IR and dye lasers. The IR laser is circularly polarized and of peak intensity $I_0 = 5.0 \times 10^{11}$ W/cm$^2$.

molecular beam affected by the focused IR deflection laser are broadened. The chromatographic resolution [27] between the undeflected and the deflected images is given by $Rs \equiv 0.589 \triangle Y_{\text{peak}}/W_{1/2} = 0.83$, where $\triangle Y_{\text{peak}}$ and $W_{1/2}$ are the distance between the peaks and the FWHM of the two images, respectively. These image shifts and a 42-$\mu$s TOF with a repeller voltage of 150 V correspond to $\triangle v_y = \pm 6.9$ m/s or an angular deflection of $\pm 0.71°$, which is equivalent to a spatial separation of $\pm 8.0$ mm for neutral $CS_2$ molecules at the detector. This suggests that a particular species of molecule could be deflected and then separated from a mixed molecular beam by placing a collector in the direction of deflection, as discussed in Ref. [25].

Deflection of the molecular beam as a function of $y$ is obtained by changing the $y$ position of the dye laser focus. Using the velocity of $CS_2$ molecules along the $z$ axis [28], $v_z(CS_2) = 560$ m/s, and IR pulse duration of $\tau = 7$ ns, the experimental data are well fitted by Eq. (3), yielding $\omega_0 = 18$ $\mu$m and $U_0 = 6.9$ meV for a circularly polarized IR laser pulse of 40 mJ. The IR laser beam used for deflection is the remaining portion of the fundamental line of Nd:YAG laser after generating the third harmonics. Scanning of the IR focus center region with a pinhole shows two Gaussian-like profiles (data not shown). The value of $\omega_0$ from fitting agrees well with that estimated from the scan result for the larger profile. After calibrating for the beam mode, the measured value of $U_0$ also agrees well with that calculated using a pulse energy of 40 mJ and the average static polarizability [29] $\alpha$ of $CS_2$, $9.6 \times 10^{-40}$ C m$^2$/V. Similar corrections are applied for the peak intensity values in this Letter.

The drastically improved resolution of the velocity map imaging technique allows us to investigate the trajectories of the molecules affected by the molecular lens in detail. The molecular ray focused by the molecular lens can be traced by measuring the image shift ($\triangle Y$) of molecules ionized at different $y$ positions as a function of the detector distance along the $z$ axis. When ionized molecules hit the detector at $t =$ TOF, neutral molecules would have flown a distance of $v_z(CS_2) \times$ TOF along the $z$ axis with the same $y$ shift as $CS_2^+$ since $\triangle v_y(CS_2) = \Delta v_y(CS_2^+)$. By varying the electrode voltages while keeping the ratio constant, the distance to the detector is scaled in proportion to the TOF of $CS_2^+$; the distance to the detector is virtually changed. Therefore, tracing of the molecular lens can be achieved by measuring $\triangle Y$ and TOF while varying the electrode voltages. Choosing an imaginary slit blocking the molecular beam with $|y_0| > \omega_0$ for convenience, the dependence of the cylindrical molecular lens properties, $W$, $D$, and $f$ on $I_0$ can be derived from Eq. (3):

$$W = 1.1\omega_0, \qquad D = 3.3\,\frac{a}{I_0}, \qquad f = \frac{a}{I_0}, \tag{4}$$

where

$$a = \frac{m\omega_0 v_z^2 \sqrt{1 + 2\ln 2[\omega_0/(v_z\tau)]^2}}{\sqrt{2\pi}\,\alpha\,\eta}, \tag{5}$$

with the vacuum impedance $\eta$. $W$ and $D$ are obtained from the intersection of molecular rays starting at $\omega_0$ ($-\omega_0$) and $-0.384\omega_0$ ($0.384\omega_0$). For experimental convenience, we measure the distance $f'$ to the intersection point of the two molecular rays with the highest deflection which pass through the molecular lens at $y = \omega_0/2$ and $-\omega_0/2$, and calculate $f$ from the relation $f = f'/e^{1/2}$. The traced molecular trajectories with $W$, $D$, and $f$ are shown in Fig. 3. Experimentally obtained values of $D$, $W$, and $f$ as a function of $1/I_0$ are plotted in Fig. 4. $W$ is independent of the peak intensity, whereas $f$ and $D$ are proportional to $1/I_0$, $f = 0.91(a/I_0)$, and $D = 2.9(a/I_0)$. In addition, the ratio of slopes for $D$ and $f$ is 3.2. These values are in excellent agreement with the theoretical prediction of Eq. (4) represented by the dashed line in Fig. 4. It is also in agreement with the prediction of Ref. [17]. As in the atomic case, a smaller $W$ is essential for high-resolution molecular lithography and for this reason, a smaller

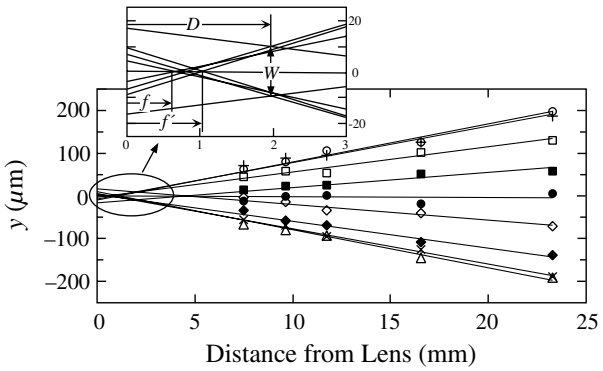


FIG. 3. Tracing of the $CS_2$ molecular rays passing through the cylindrical molecular lens of width $2\omega_0 = 36$ $\mu$m. The IR laser is circularly polarized with $I_0 = 3.6 \times 10^{11}$ W/cm$^2$. The inset box shows the characteristic lens parameters obtained from the extrapolation of the tracing results. Each set of data with the same symbol represents the trajectory of molecules starting from the same point. Lines are the least-squares fits. Horizontal scale is the distance from the lens traveled by neutral molecules during TOF given by the product $v_z(CS_2) \times$ TOF($CS_2^+$).

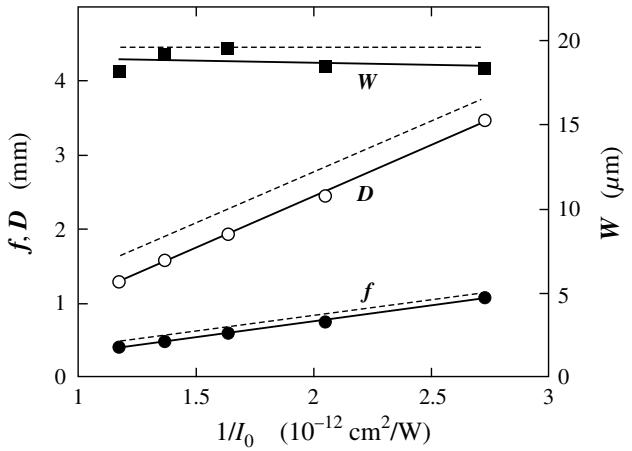


FIG. 4. Intensity dependence of the molecular lens parameters. Solid lines are fits of the experimental results for each of the parameters, and dashed lines are the theoretical predictions.

value of $a/I_0$ is preferred. Even for a far-off-resonance frequency, however, multiphoton ionization limits the maximum intensity of the deflecting laser thus limiting the minimum value of $a/I_0$. Although it is difficult to reduce $a/I_0$ further, it is possible to reduce $W$ by lowering the aperture size for the molecular beam and subsequently eliminating the spherical aberrations ($f \approx D$).

In conclusion, we have obtained the first 2D images of molecules spatially separated by a cylindrical molecular lens. This molecular lens is based on the optical dipole force which is exerted by the interaction between the laser field and the induced dipole moment of the molecules. We obtained characteristic lens parameters including the focal length, minimum beam width, and distance to the minimum-width position by tracing the trajectories of the deflected molecules from the ion images and TOFs as a function of the electrode voltages. It opens up exciting possibilities for novel components in molecular optics and a new type of optical chromatography for separating a particular molecule from a mixture.

This work was supported by CRI and NRL, the Ministry of Science and Technology, Korea.

*Corresponding author.
Email address: dschung@snu.ac.kr

[1] A. Ashkin, Phys. Rev. Lett. **24**, 156 (1970).
[2] S. Chu, Science **253**, 861 (1991).
[3] T. T. Perkins *et al.,* Science **264**, 822 (1994).
[4] A. Ashkin *et al.,* Nature (London) **348**, 346 (1990).
[5] J. T. Finer, R. M. Simmons, and J. A. Spudich, Nature (London) **368**, 113 (1994).
[6] A. Ashkin and J. M. Dziedzic, Science **235**, 1517 (1987).
[7] S. Chu *et al.,* Phys. Rev. Lett. **57**, 314 (1986).
[8] M. H. Anderson *et al.,* Science **269**, 198 (1995).
[9] D. S. Weiss, B. C. Young, and S. Chu, Phys. Rev. Lett. **70**, 2706 (1993).
[10] J. J. McClelland *et al.,* Science **262**, 877 (1993).
[11] A. Hemmerich and T. W. Hänsch, Phys. Rev. Lett. **70**, 410 (1993).
[12] W. Demtröder, *Laser Spectroscopy: Basic Concepts and Instrumentation* (Springer-Verlag, New York, 1996).
[13] H. Stapelfeldt *et al.,* Phys. Rev. Lett. **79**, 2787 (1997).
[14] H. Sakai *et al.,* Phys. Rev. A **57**, 2794 (1998).
[15] B. Friedrich and D. Herschbach, Phys. Rev. Lett. **74**, 4623 (1995).
[16] J. Karczmarek *et al.,* Phys. Rev. Lett. **82**, 3420 (1999).
[17] T. Seideman, J. Chem. Phys. **106**, 2881 (1997).
[18] T. Seideman, J. Chem. Phys. **111**, 4397 (1999).
[19] T. Takekoshi, B. M. Patterson, and R. J. Knize, Phys. Rev. Lett. **81**, 5105 (1998).
[20] A. N. Nikolov *et al.,* Phys. Rev. Lett. **82**, 703 (1999).
[21] H. Sakai *et al.,* J. Chem. Phys. **110**, 10 235 (1999).
[22] R. A. Morgan *et al.,* J. Chem. Phys. **104**, 6117 (1996).
[23] D. H. Parker and A. T. J. B. Eppink, J. Chem. Phys. **107**, 2357 (1997).
[24] A. T. J. B. Eppink and D. H. Parker, Rev. Sci. Instrum. **68**, 3477 (1997).
[25] T. Seideman, J. Chem. Phys. **107**, 10 420 (1997).
[26] P. S. Pershan, J. P. van der Ziel, and L. D. Malmstrom, Phys. Rev. **143**, 574 (1966).
[27] D. C. Harris, *Exploring Chemical Analysis* (W. H. Freeman and Company, New York, 1997).
[28] D. R. Miller, in *Atomic and Molecular Beam Methods,* edited by G. Scoles (Oxford University Press, New York, 1988), p. 15.
[29] K. J. Miller, J. Am. Chem. Soc. **112**, 8543 (1990).